Research Article | Vol. 34, No. 3 / March 2017 / Journal of the Optical Society of America B 601

Journal of the Optical Society of America B
OPTICAL PHYSICS

High repetition rate mid-infrared supercontinuum generation from 1.3 to 5.3 μm in robust step-index tellurite fibers

Stefan Kedenburg,[1,†,*] Clément Strutynski,[2,†] Bertrand Kibler,[2,3] Paul Froidevaux,[2] Frédéric Désévédavy,[2] Grégory Gadret,[2] Jean-Charles Jules,[2] Tobias Steinle,[1] Florian Mörz,[1] Andy Steinmann,[1] Harald Giessen,[1] and Frederic Smektala[2]

[1]4th Physics Institute and Research Center SCOPE, University of Stuttgart, 70550 Stuttgart, Germany
[2]Laboratoire Interdisciplinaire Carnot de Bourgogne, UMR 6303 CNRS-UBFC, 9 Av. Alain Savary, BP 47870, 21078 Dijon, France
[3]e-mail: bertrand.kibler@u-bourgogne.fr
*Corresponding author: s.kedenburg@pi4.uni-stuttgart.de

Received 1 November 2016; revised 19 January 2017; accepted 24 January 2017; posted 24 January 2017 (Doc. ID 279893); published 22 February 2017

We demonstrate broadband supercontinuum generation over two infrared octaves, spanning from 1.3 to 5.3 μm, with an output power of 150 mW in robust step-index tellurite fibers with core diameters between 3.5 and 4.3 μm. As a pump source, we use femtosecond mid-IR pulses from a home-built post-amplified optical parametric oscillator tunable between 1.5 and 4.0 μm at a 43 MHz repetition rate. We study the influence of core size, pump wavelength, and fiber length to optimize the spectral bandwidth. A key requirement for efficient spectral broadening is a low and rather flat average anomalous dispersion over a wide spectral range that can be tailored accordingly by changing the fiber core diameter. Numerical simulations based on the generalized nonlinear Schrödinger equation are in good agreement with experimental results.

OCIS codes: (060.4370) Nonlinear optics, fibers; (160.4330) Nonlinear optical materials; (320.6629) Supercontinuum generation.

https://doi.org/10.1364/JOSAB.34.000601

1. INTRODUCTION

In recent years, strong efforts have been undertaken to transfer robust high brightness supercontinuum (SC) sources from visible and near-infrared into the mid-infrared spectral range [1]. In particular, alternative materials to fused silica were utilized based on fluoride, tellurite, and chalcogenide fibers [2,3]. A key requirement for practical applications, such as spectroscopy, is a high repetition rate in the MHz range that enables higher average output powers, shorter acquisition times due to a better signal-to-noise ratio compared to pump systems with low kHz repetition rates [4,5], and low numbers of pulses per pixel.

An advantage of fluoride fibers, such as fluorozirconate (ZBLAN) or fluoroindate (InF_3), is a low material zero dispersion wavelength (ZDW) of ∼1.6 μm, which is beneficial for anomalous dispersion pumping with commonly available laser sources [6–9]. However, fluoride glass possesses a low nonlinear refractive index that is comparable to that of fused silica, whereas chalcogenide fibers [10–15], such as As_2S_3 or As_2Se_3, exhibit approximately 2 to 3 orders of magnitude higher nonlinear refractive indices. Furthermore, chalcogenide glasses have broad transmission windows up to 15 μm [16,17], exceeding that of fluorides and tellurite glasses, which are limited to ∼5 μm. Nevertheless, tellurium oxide-based glasses are a good compromise for SC generation in the mid-infrared because they exhibit higher nonlinear refractive indices than fluorides (∼10 times) and superior optical damage thresholds, as well as lower ZDWs compared to chalcogenide glasses.

Several demonstrations in tellurite fibers have been based on microstructured fibers with small core sizes to further enhance the nonlinearity and to down-shift the ZDW below 2 μm, allowing for anomalous dispersion pumping with conventional laser sources [18–22]. However, most of the previous works report limited spectral coverage above 3 μm due to increased absorption related to water retention and a reduced damage threshold, which hinders further power scaling. The broadest bandwidth to date was obtained by Domachuk *et al.* [22] with an output spectrum spanning from 0.8 to 4.8 μm at a power level of 70 mW. Nonetheless, the power proportion in the mid-IR regions remains limited because of a pump wavelength near 1.5 μm. Some recent works with robust, low-loss W-index fibers have demonstrated that coverage of the important atmospheric transmission window between 3 and 5 μm with simultaneously high output powers is feasible [23,24].

In this work, we have enhanced the SC bandwidth in the mid-infrared (1.3–5.3 μm) with an engineered dispersion profile of our robust step-index tellurite fiber and, importantly, achieved at the same time a high output power of 150 mW. A detailed experimental and numerical parameter study on the spectral behavior is presented based on pumping with mid-IR femtosecond pulses at a MHz repetition rate.

2. STEP-INDEX TELLURITE FIBER PROPERTIES

Quasi-single-mode step-index tellurite fibers are fabricated with a combination of built-in casting and rod-in-tube techniques, described in detail in a previous work [25]. Development of such multi-material fibers implies the co-drawing of different glasses with matching thermo-mechanical properties as well as adequate refractive index values [26]. Thus, the following tailored glass composition percentages were selected: $80TeO_2$-5ZnO-$10Na_2O$-$5ZnF_2$ (TZNF) for the core and $60TeO_2$-$20Na_2O$-$15GeO_2$-5ZnO (TNaGZ) for the cladding. To ensure minimum contamination from OH compounds, the synthesis and shaping of the glass preforms were performed under a dry atmosphere (dry glove box). In addition, the use of zinc fluoride in the core material composition enables further reduction of hydroxyl-related absorptions in the mid-IR [27,28]. A preform was synthesized from these compositions and drawn into a large-core fiber, whose attenuation spectrum is shown in Fig. 1(a). The glass OH content is very low (<0.5 ppm [25]), and the water related absorption band between 3 and 4 μm is nearly completely eliminated. However, an accurate loss measurement was not possible beyond 4 μm. Small-core fibers were then prepared from the same initial preform by jacketing this preform with a second cladding tube of the same cladding composition (TNaGZ) [25].

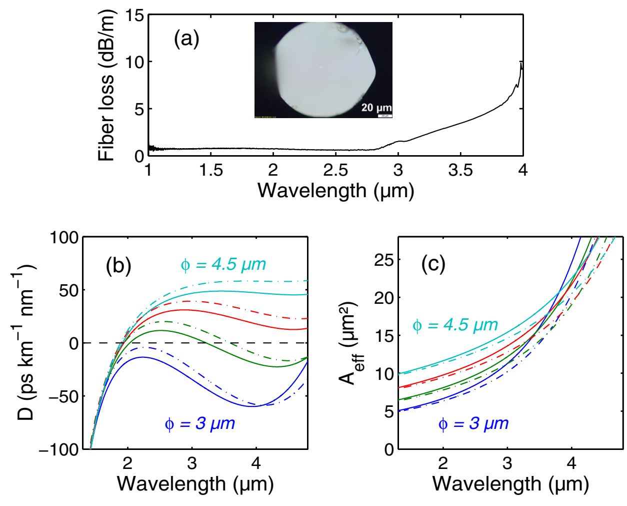

Fig. 1. (a) Measured fiber losses of a large-core step-index TZNF/TNaGZ fiber determined by the cutback technique (inset: image of a small-core fiber cross section). A 10-m-long fiber was cut every 30–40 cm. (b),(c) Wavelength-dependent dispersion D and effective mode area A_{eff}, respectively, of the fundamental guided mode in our step-index tellurite fiber with varying core diameters: $\phi = 3, 3.5, 4$, or 4.5 μm. Solid and dashed lines indicate the resulting uncertainty due to the fitting procedure of refractive index difference for our glass pair.

As reported below, the variation of the core diameter enables management of fiber dispersion properties to enhance SC generation.

The wavelength-dependent refractive index curve for both core and cladding glasses was obtained with different interpolation schemes based on two-pole Sellmeier equations to fit previous near-IR measurements reported in Ref. [25,29]. However, it is worth mentioning that the resulting refractive index difference for our TZNF/TNaGZ glass pair in the mid-infrared has to be considered cautiously (see Ref. [29]). Consequently, in the following numerical study, some uncertainty range is introduced in the step-index profile to better reveal the potential dispersion fiber properties. For instance, the core-cladding index difference varies between 0.103 and 0.116 at 2 μm. Based on our simple step-index profile, we then studied the corresponding modal properties of our tellurite fiber with various core diameters by numerically solving the dispersion equation (also called the eigenvalue equation) for cylindrical step-index waveguides. Figures 1(b) and 1(c) report dispersion curves and the effective mode area, respectively, as a function of wavelength for the fundamental guided mode. For a core diameter ranging from 3 to 4.5 μm, we observe that our fiber can exhibit distinct dispersive properties such as an all-normal dispersion profile or even a multi-ZDW dispersion profile [see Fig. 1(b)]. The presence of an all-normal dispersion regime appears for core diameters ϕ below 3–3.25 μm. The first and second ZDWs can be easily shifted from 1.9 to 2.3 μm and from 2.8 to 4 μm, respectively. For the particular choice of core diameter around 3.5–3.75 μm, our tellurite fiber can exhibit a low and rather flat dispersion over a wide spectral bandwidth from 2 to 5 μm. We also notice that such small core diameters imply that the effective mode area significantly spreads into the cladding for wavelengths beyond 3–4 μm [i.e., strong dispersion of $A_{\mathrm{eff}}(\lambda)$]. Nevertheless, the optical confinement proves rather efficient in the 2–3 μm range, close to that obtained in previous microstructured fibers [30]. Note also that our small-core fibers used here are not strictly single-mode for near-IR wavelengths when calculating the V number; however, only the fundamental mode was excited in our experiments. Depending on the core diameter, only a few higher order modes can exist for wavelengths beyond 1.5 μm due to typical high confinement losses [29].

3. NUMERICAL SIMULATIONS

In the following, we numerically investigate the optimization of fiber parameters for SC generation with mid-IR femtosecond pulses, especially the SC bandwidth and extension toward the mid-infrared. The objective is to roughly determine the range of parameters suitable for optimized SC generation due to possible uncertainty in the dispersion curve and mid-IR losses of our small-core fibers. To this end, we performed numerical simulations of the nonlinear pulse propagation in our step-index tellurite fibers with different core diameters and pumping parameters (250-fs pulses tunable from 1.8 to 2.8 μm with 6-kW peak power), similar to the laser properties used in the later experimental work. Our simulations used a generalized nonlinear Schrödinger equation that considered the full dispersion curve, both instantaneous and delayed nonlinear responses, and also the dispersion of nonlinearity [31]. The nonlinear Kerr coefficient is deduced from numerical calculation of the effective mode area and the nonlinear refractive index $n_2 = 3.8 \cdot 10^{-19}\ \mathrm{m}^2\ \mathrm{W}^{-1}$ [21]. For the Raman response function, we used an intermediate-broadening model using convolutions of the Lorentzian and Gaussian functions adapted from spontaneous Raman scattering spectra and estimated Raman gain coefficient given in Ref. [32]. The contribution of the delayed Raman response $f_R = 0.25$ was then deduced from the above analysis. Our model also includes the fiber losses in the 1–4 μm spectral range measured in Fig. 1(a) and extrapolation above 4 μm (i.e., the multi-phonon absorption edge).

Figure 2 summarizes the impact of both the fiber core diameter (i.e., fiber dispersion) and the pump wavelength on the expected output SC. Here the numerical results are based on both dispersion and mode area curves shown with solid lines in Figs. 1(b) and 1(c). Additional simulations were performed with fiber properties shown with dashed lines, and they lead to the same conclusions reported below. Our study considers a core diameter ranging from 3 to 4.2 μm with steps of 25 nm and a pump wavelength ranging from 1.8 to 2.8 μm with steps of 25 nm. The fiber length was fixed at 10 cm. As the largest SC frequency bandwidth expressed in THz does not always correspond to the highest mid-infrared wavelength reached, Figs. 2(a) and 2(c) show those two SC parameters, respectively.

Figure 2(b) presents the spectral flatness criterion, which is another fundamental property of SC performance (i.e., constant power spectral density along the SC spectrum). Typically, values of spectral flatness above 0.6 correspond to narrow or less than 20 dB power fluctuations over the SC bandwidth. From Fig. 2(a), we infer that when pumping in the normal dispersion regime ($\phi < 3.25$ μm), the spectral broadening is clearly limited to a few tens of THz, and extension in the mid-IR is also inhibited [see Fig. 2(c)]. Indeed, SC generation is mainly driven by self-phase modulation and optical wave-breaking, and it remains nearly symmetric and flat around the pump wavelength [see Fig. 2(b); the SC flatness is not far from the maximum value of 1]. Note that asymmetric spectra can be observed, as the wave-breaking process is sensitive to the dispersion slope. Another clear situation of less flat SC is given when considering pumping fibers with rather large anomalous dispersion ($\lambda_p > 2500$ nm and $\phi > 3.8$ μm). Then spectral broadening is fully driven by soliton dynamics and Raman soliton-self-frequency shift. The presence of a ZDW also induces the formation of dispersive waves in normal dispersion, in the near-IR largely below 2000 nm. This favors the development of wide SC bandwidth, as shown in Fig. 2(a), but SC flatness is very low because emerging solitons and phase-matched dispersive waves are initially far from the ZDW and from each other, drastically limiting frequency conversion and power spectral density in the spectral region around the ZDW ($\lambda \sim 1800$–2300 nm).

Next, we retrieve the usual case of the optimization of SC bandwidth and flatness, which consists of pumping the fiber close to the corresponding ZDW [31]. However, note that for large core diameters ($\phi > 3.8$ μm), this corresponds to pump wavelengths below 2500 nm, and the mid-IR extension of SC remains limited due to large anomalous dispersion (and even lower nonlinearity) experienced by Raman shifted-solitons in the mid-IR. Finally, the optimized parameters for SC generation (i.e., large bandwidth, sufficient flatness, and extension into the mid-IR) in our tellurite fibers are a pump wavelength between 2200 and 2600 nm, and a fiber core diameter between 3.4 and 3.7 μm. When inspecting the corresponding fiber properties in Fig. 1, such conditions correspond to the pumping of fibers with low and rather flat dispersion (even with multiple ZDWs) over a large spectral range. Raman soliton-self-frequency shift can then be enhanced, and even if a second ZDW is present, mid-IR red-shifted dispersive waves are further generated. Even with a moderate input peak power for femtosecond pulses (here 6 kW), our simulations reveal that a rather flat SC covering the 1400–5000 nm range (~150 THz) can be obtained. Extensive SC simulations, taking into account the uncertainty of predicted fiber properties (see Fig. 1), indicate that SC optimization could be obtained for core diameters between 3.3 and 3.6 μm. It is worth mentioning that the fiber length studied here allowed us to observe the overall SC development without too many limitations related to the fiber losses, except beyond 5 μm, since the multi-phonon absorption edge is already reached. For longer fibers, the maximum mid-IR SC extension [see Fig. 2(c)] is found to

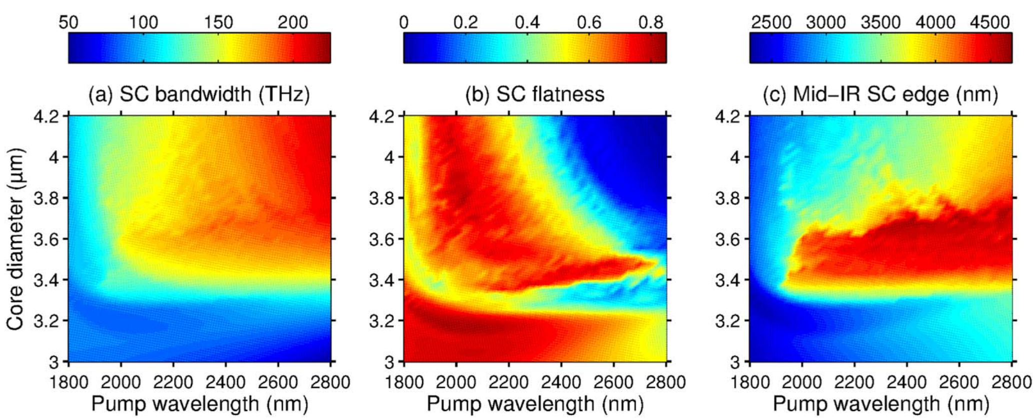

Fig. 2. Numerical investigation of the impact of both the fiber core diameter ϕ and the pump wavelength λ_p on (a) the expected output SC bandwidth at −20 dB expressed in THz, (b) the expected SC flatness (for definition see text), and (c) the expected SC mid-IR wavelength edge.

continuously decrease, for example, toward 4200 nm for a 1-m-long fiber segment. Similar findings were already demonstrated for SC generation in short segments of silica fibers where the mid-IR SC extension can reach 3 μm (i.e., the multi-phonon absorption edge, since the fiber loss approaches 100 dB/m at such wavelengths) [33]. Our analysis of the spectral broadening mechanisms and associated SC generation performance confirms the key role of an engineered dispersion profile even for a simple step-index tellurite fiber. This can also minimize the costly and time-consuming experimental trial and error approach reported below as a proof-of-principle demonstration.

4. EXPERIMENTAL SETUP

The setup implemented for experimental SC demonstrations is schematically illustrated in Fig. 3. The pump source is based on a post-amplified fiber-feedback optical parametric oscillator (OPO), which delivers gap-free tunability between 1.5 and 2.0 μm (signal) and 2.2–4.0 μm (idler) with watt-level output power [34,35]. A home-built 7 W, 450 fs Yb:KGW oscillator at a repetition rate of 43 MHz [36] was used to pump the OPO, as well as the subsequent optical parametric amplifier (OPA). The signal pulses from the OPO with durations of 300–500 fs at full width at half maximum and average powers of about 200 mW were utilized as seeds for the OPA. Both the OPO and the OPA employed a periodically-poled lithium tantalate crystal as a nonlinear gain medium to obtain the highest output powers in an idler wavelength range around 2.4 μm [35]. The IR pump power was controlled by varying the OPA pump power and thus the gain of the OPA unit. The signal and idler pulse durations of the OPA are measured to be in the same range as of the OPO (250–350 fs for the 1.5–3.2 μm range under study in the following) [34]. Signal and idler pulses were coupled into and collimated after the tellurite fibers via C-and E-antireflection coated aspherical lenses from Newport and Thorlabs, respectively. The total transmission efficiencies of the signal wavelengths decrease from approximately 65% to about 40% for longer wavelengths, mainly due to the increasing losses of the lenses above 1800 nm. For the idler, the total transmission peaked at a wavelength of 2600 nm with approximately 45%, sharply decreasing to about 10% above 3000 nm due to the rising material absorption in the tellurite fibers. In addition, the pump wavelength with a smaller core diameter of 3.5 μm compared to the 4.3 μm fiber core diameter leads to slightly (∼5–10%) decreased transmission efficiencies. To optimize the beam shape and ensure a good beam quality (mostly single-mode operation), an IR-camera (Pyrocam 3, Spiricon) was used. The SC output was free-space-coupled and recorded in a Fourier transform infrared spectrometer (Frontier FTIR spectrometer, Perkin Elmer, range 1.3–25 μm).

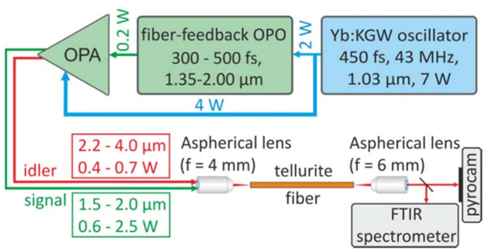

Fig. 3. Experimental setup. A home-built Yb:KGW oscillator was used to pump a fiber-feedback OPO whose signal pulses were applied to seed an OPA. Both signal (1.5–2.0 μm) and idler (2.2–4.0 μm) of the post amplifier were used to couple into the step-index tellurite fibers via an aspherical lens. Coupling into the 3.5–4.3 μm large cores was ensured by imaging the fiber end faces onto a pyro-camera with an aspherical lens. The spectra were recorded with an FTIR spectrometer.

5. EXPERIMENTAL RESULTS

Our experiments consist of three parameter studies to investigate the impacts of the fiber core diameter, the pump wavelength, and the fiber length on SC generation, thus revealing the best conditions to obtain an efficient broadband light source in the mid-infrared spectral region.

A. Variation of Core Diameter

In Fig. 4, three different core diameter sizes of (a) 3.5, (b) 3.8, and (c) 4.3 μm are illustrated for the same pump wavelength of 2400 nm, with fixed fiber lengths of around 9 cm and nearly constant coupled peak power of ∼6 kW. Due to increased anomalous dispersion [see Fig. 1(b)] in combination with larger effective mode areas, the spectral bandwidth decreases with larger core diameter. The output power is only slightly affected by the core size and is ∼70 mW. This confirms that losses are similar for all fibers. For the 1.5–3 μm spectral region, the losses of such small-core fibers were also confirmed to be close to those measured in Fig. 1 [29].

We achieved the broadest spectrum spanning from about 2 to 5 μm (−20 dB bandwidth) in the mid-infrared by using the 3.5 μm core fiber. The strong impact of a low and rather flat dispersion curve in the anomalous dispersion regime for efficient coverage of the long-wavelength range is confirmed to be crucial as previously revealed by our simulations. Here, we can note that the low dynamic range of our spectral measurements does not allow us to effectively simultaneously show the overall SC bandwidth (due to our free-space-coupling

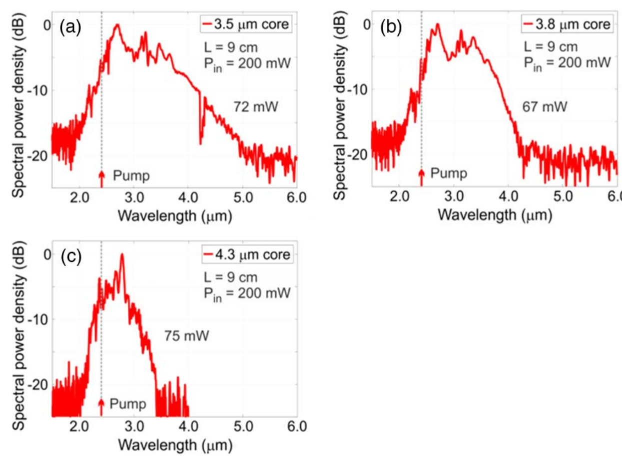

Fig. 4. Experimental SC spectra for distinct fibers with core diameters equal to (a) 3.5, (b) 3.8, and (c) 4.3 μm, and pumped at 2.4 μm with a constant coupled peak power of ∼6 kW. The fiber lengths remained fixed at around 9 cm. The average output power is given for each SC spectrum.

condition in the FTIR), in particular, for possible weaker DWs at wavelengths below 2 μm. Since collimation of a spectral broadband beam is difficult, we recorded several spectra for slightly different positions of the collimation lens and then averaged them.

B. Variation of Pump Wavelength

1. Signal Wavelengths

The spectral broadening at a constant incoming power of 200 mW (i.e., measured after IR objective as the coupling efficiency varies) for different wavelengths in the range between 1500 and 1975 nm are shown in Fig. 5. The investigated tellurite fiber was 9 cm long and had a core diameter of 3.5 μm. In this wavelength range, we pump exclusively in the normal dispersion regime. The SC spectra are typically flat with a narrow bandwidth [see Figs. 2(a) and 2(b)]. The SC bandwidth increases for longer wavelengths due to a pumping condition closer to the first ZDW (around 2 μm) and the subsequent formation of solitons in the anomalous dispersion. The output power shrinks from 138 mW at 1500 nm to 58 mW at 1975 nm mainly due to the increased losses at the coupling lenses. The broadest spectrum at a pump wavelength of 1975 nm covers the 1.6 to 2.4 μm range. At a signal wavelength of 1700 nm, the spectral bandwidth is clearly narrower due to an increased pulse width of the OPA at this specific wavelength.

2. Idler Wavelengths

Similar to the case of the signal wavelengths, the impact of the idler pump wavelengths on the spectral bandwidth is characterized for constant incoming powers of 200 mW, a fixed fiber length of 9 cm, and a core diameter of 3.5 μm. The six idler wavelengths, each represented by a different color, range between 2.2 and 3.2 μm, as depicted in Fig. 6.

The broadest SC bandwidth with long mid-IR extension is generated when pumped between 2.4 and 2.8 μm, similarly to

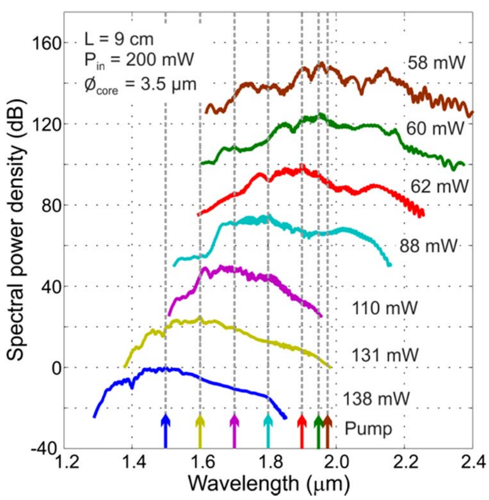

Fig. 5. Experimental SC spectra for various signal pump wavelengths between 1.5 and 2.0 μm (see colored arrows) generated in the tellurite fiber with a core diameter of 3.5 μm at a constant incoming power of 200 mW. The fiber length remained fixed at 9 cm. For better visibility, the spectra were shifted apart by 25 dB. The average output power is given for each SC spectrum.

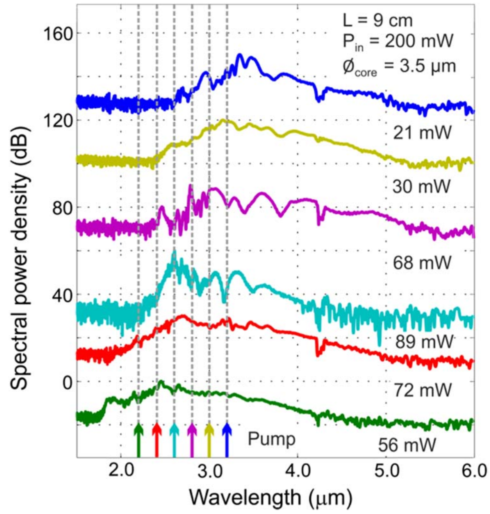

Fig. 6. Experimental SC spectra for various idler pump wavelengths between 2.2 and 3.2 μm (see colored arrows) generated in the tellurite fiber with a core diameter of 3.5 μm at constant incoming power of 200 mW. The fiber length remained fixed at 9 cm. The spectral dips observed around 4.2 μm came from CO_2 absorptions during the free space coupling of the SC output into the FTIR. For better visibility, the spectra were shifted apart by 30 dB. The average output power is given for each SC spectrum.

our numerical predictions. We also notice that the long-wavelength edge is set by strong material absorption in the tellurite glass to ∼5.3 μm. This upper limit cannot be further increased for longer pump wavelengths. The SC flatness is optimized for shorter pump wavelengths between 2.2 and 2.4 μm, remaining close to the first ZDW. The short-wavelength edge shifts, but it appears difficult to evaluate the genuine position due to our limited dynamic range. The output power peaked for the 2600 nm pump with a magnitude of 89 mW due to an increased loss of the lenses for shorter wavelengths and because of rising material absorption in the tellurite fiber [see Fig. 1(a)] for longer wavelengths. However, the 2.6 μm idler wavelength (corresponding to a signal wavelength of 1700 nm) results in a clearly narrower spectrum that can be explained by strong atmospheric absorptions degrading the pulse spectrum of the OPA.

C. Variation of Fiber Length

A set of different spectra generated in fiber lengths between 6 and 12 cm are displayed in Fig. 7. From previous measurements, we chose the optimized pump wavelength at 2400 nm and the tellurite fiber with a 3.5-μm core diameter. Here we determine the maximum incoming power of our laser source to be equal to 400 mW. The optimum fiber length of 9 cm is experimentally demonstrated, leading to a supercontinuum with a record spectral coverage in tellurite glass fibers in the mid-infrared from 1.3 to 5.3 μm [see spectrum in Fig. 7(b)]. The achieved output power of 150 mW is rather high due to the high repetition rate of 43 MHz, particularly when compared to kHz systems. The upper wavelength limit is given by the multi-phonon absorption edge of the tellurite glass around 5 μm, and it could not be substantially increased

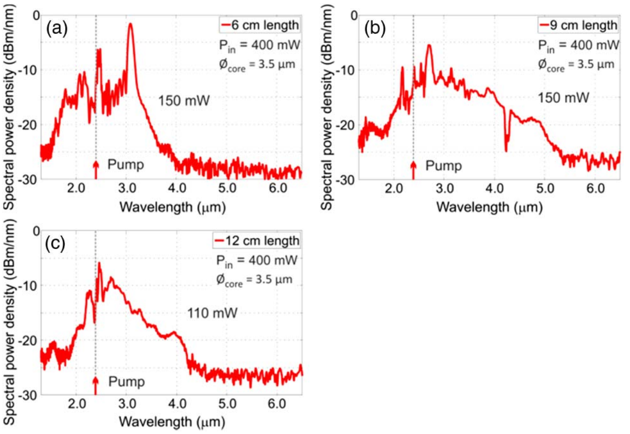

Fig. 7. Experimental SC spectra obtained for various fiber lengths, (a) 6, (b) 9, and (c) 12 cm, of the tellurite fiber with a core diameter of 3.5 μm pumped at 2.4 μm with a constant incoming power of 400 mW. The average output power is given for each SC spectrum.

by the generation of red-shifted dispersive waves compared to pumping with input powers of 200 mW. However, the measured short-wavelength edge could be shifted from approximately 2.0 to about 1.3 μm due to the formation of stronger blue-shifted dispersive waves in the normal dispersion regime. For the 6- and 12-cm-long fibers, the spectral bandwidth is significantly reduced. In particular, soliton self-frequency shift and dispersive wave dynamics are not fully developed for the 6-cm-long fiber segment, whereas mid-IR fiber loss could be the limiting factor for the 12-cm-long segment. Note that the mid-IR SC extension is experimentally found to be more sensitive to fiber length than in our simulations (a similar impact of multi-phonon absorption edge was observed in Sec. 3 with further propagation about a few tens of cm). High absorption losses in this spectral region (beyond 4 μm) can be related to the multi-phonon absorption of the tellurite glass and also to the fact that effective mode area significantly spreads into the cladding for these wavelengths, thus leading to possible confinement losses or scattering due to interface defects into the cladding (introduced during jacketing the first preform with a second cladding).

Here, the broadband SC output spanning over two infrared octaves in the 9-cm-long fiber with a core diameter of 3.5 μm is significantly boosted by the engineered dispersion curve in this spectral region. With lower absorption losses in the wavelength range between 4 and 5 μm, even flatter SC may be realized in the future. Our femtosecond pump pulses at 2.4 μm are efficiently converted into novel spectral components, leading to a high power proportion (about 45%) of the supercontinuum in the 3–5 μm atmospheric window.

6. CONCLUSION

An extensive numerical and experimental study of SC generation was performed in robust dispersion-engineered step-index tellurite fibers, in particular, by changing the core diameter, pump wavelength, and fiber length. The pump source was based on a recently developed post-amplified fiber-feedback OPO that delivers tunable femtosecond pulses at wavelengths from 1.5 to 4.0 μm with a 43 MHz repetition rate. The pump system was optimized for enhanced performance in the 2.1–2.5 μm range compared to a recent publication [24]. We achieved an infrared spectral bandwidth of over 4000 nm spanning from 1.3 to 5.3 μm when a 9-cm-long segment of 3.5-μm core tellurite fiber was pumped at 2400 nm. This is, to the best of our knowledge, the broadest supercontinuum in the mid-infrared obtained in tellurite fibers. The enhancement in spectral broadening compared to recent publications is mainly attributed to the low and rather flat dispersion (even with multiple ZDWs) associated with an optimized pump wavelength. The long-wavelength edge of the SC is here limited by the intrinsic transmission window of the tellurite glass. The achieved output average power is 150 mW with about 45% power proportion in the important transparent 3 to 5 μm atmospheric window. Further power scalability due to the excellent mechanical properties of the step-index tellurite fiber is possible. Our results make step-index tellurite fibers suitable candidates for the next generation of nonlinear photonic devices in the important spectral region from 2 to 5 μm, in particular, to take advantage of the recent development of ultrashort pulse lasers sources beyond 2 μm.

Funding. European Research Council (ERC) (Complexplas); Deutsche Forschungsgemeinschaft (DFG) (SPP1391, FOR730, GI 269/11-1); Bundesministerium für Bildung und Forschung (BMBF) (13N9048, 13N10146, Printoptics); Carl-Zeiss-Stiftung; Baden-Württemberg Stiftung (Spitzenforschung 2); Agence Nationale de la Recherche (ANR) (ANR-13-BS08-0008, ANR-11-LABX-0001-01); Direction Générale de l'Armement (DGA); Conseil Regional de Bourgogne.

Acknowledgment. Support was received from the Direction Générale de l'Armement through a DGA-MRIS scholarship.

[†]These authors contributed equally to this work.

REFERENCES

1. J. Swiderski, "High-power mid-infrared supercontinuum sources: current status and future perspectives," Prog. Quantum Electron. **38**, 189–235 (2014).
2. G. Tao, H. Ebendorff-Heidepriem, A. M. Stolyarov, S. Danto, J. V. Badding, Y. Fink, J. Ballato, and A. F. Abouraddy, "Infrared fibers," Adv. Opt. Photon. **7**, 379–458 (2015).
3. Y. Yu, X. Gai, T. Wang, P. Ma, R. Wang, Z. Yang, D.-Y. Choi, S. Madden, and B. Luther-Davies, "Mid-infrared supercontinuum generation in chalcogenides," Opt. Mater. Express **3**, 1075–1086 (2013).
4. C. Wei, X. Zhu, R. A. Norwood, F. Song, and N. Peyghambarian, "Numerical investigation on high power mid-infrared supercontinuum fiber lasers pumped at 3 μm," Opt. Express **21**, 29488–29504 (2013).
5. T. Steinle, F. Neubrech, A. Steinmann, X. Yin, and H. Giessen, "Mid-infrared Fourier-transform spectroscopy with a high-brilliance tunable laser source: investigating sample areas down to 5 μm diameter," Opt. Express **23**, 11105–11113 (2015).
6. W. Yang, B. Zhang, G. Xue, K. Yin, and J. Hou, "Thirteen watt all-fiber mid-infrared supercontinuum generation in a single mode ZBLAN fiber pumped by a 2 μm MOPA system," Opt. Lett. **39**, 1849–1852 (2014).

7. R. Salem, Z. Jiang, D. Liu, R. Pafchek, D. Gardner, P. Foy, M. Saad, D. Jenkins, A. Cable, and P. Fendel, "Mid-infrared supercontinuum generation spanning 1.8 octaves using step-index indium fluoride fiber pumped by a femtosecond fiber laser near 2 μm," Opt. Express **23**, 30592–30602 (2015).
8. J.-C. Gauthier, V. Fortin, J.-Y. Carrée, S. Poulain, R. Vallée, and M. Bernier, "Mid-IR supercontinuum from 2.4 to 5.4 μm in a low-loss fluoroindate fiber," Opt. Lett. **41**, 1756–1759 (2016).
9. X. Jiang, N. Y. Joly, M. A. Finger, F. Babic, G. K. L. Wong, J. C. Travers, and P. St.J. Russell, "Deep-ultraviolet to mid-infrared supercontinuum generated in solid-core ZBLAN photonic crystal fibre," Nat. Photonics **9**, 133–139 (2015).
10. B. Zhang, Y. Yu, C. Zhai, S. Qi, Y. Wang, A. Yang, X. Gai, R. Wang, Z. Yang, and B. Luther-Davies, "High brightness 2.2–12 μm mid-infrared supercontinuum generation in a nontoxic chalcogenide step-index fiber," J. Am. Ceram. Soc. **99**, 2565–2568 (2016).
11. R. R. Gattass, L. B. Shaw, V. Q. Nguyen, P. C. Pureza, I. D. Aggarwal, and J. S. Sanghera, "All-fiber chalcogenide-based mid-infrared supercontinuum source," Opt. Fiber Technol. **18**, 345–348 (2012).
12. S. Kedenburg, T. Steinle, F. Mörz, A. Steinmann, and H. Giessen, "High-power mid-infrared high repetition-rate supercontinuum source based on a chalcogenide step-index fiber," Opt. Lett. **40**, 2668–2671 (2015).
13. S. Xie, N. Tolstik, J. C. Travers, E. Sorokin, C. Caillaud, J. Troles, P. St.J. Russell, and I. T. Sorokina, "Coherent octave-spanning mid-infrared supercontinuum generated in As_2S_3-silica double-nanospike waveguide pumped by femtosecond Cr:ZnS laser," Opt. Express **24**, 12406–12413 (2016).
14. U. Møller, Y. Yu, I. Kubat, C. R. Petersen, X. Gai, L. Brilland, D. Méchin, C. Caillaud, J. Troles, B. Luther-Davies, and O. Bang, "Multi-milliwatt mid-infrared supercontinuum generation in a suspended core chalcogenide fiber," Opt. Express **23**, 3282–3291 (2015).
15. O. Mouawad, J. Picot-Clémente, F. Amrani, C. Strutynski, J. Fatome, B. Kibler, F. Désévédavy, G. Gadret, J.-C. Jules, D. Deng, Y. Ohishi, and F. Smektala, "Multioctave midinfrared supercontinuum generation in suspended-core chalcogenide fibers," Opt. Lett. **39**, 2684–2687 (2014).
16. C. R. Petersen, U. Møller, I. Kubat, B. Zhou, S. Dupont, J. Ramsay, T. Benson, S. Sujecki, N. Abdel-Moneim, Z. Tang, D. Furniss, A. Seddon, and O. Bang, "Mid-infrared supercontinuum covering the 1.4–13.3 μm molecular fingerprint region using ultra-high NA chalcogenide step-index fibre," Nat. Photonics **8**, 830–834 (2014).
17. T. Cheng, K. Nagasaka, T. H. Tuan, X. Xue, M. Matsumoto, H. Tezuka, T. Suzuki, and Y. Ohishi, "Mid-infrared supercontinuum generation spanning 2.0 to 15.1 μm in a chalcogenide step-index fiber," Opt. Lett. **41**, 2117–2120 (2016).
18. I. Savelii, O. Mouawad, J. Fatome, B. Kibler, F. Désévédavy, G. Gadret, J.-C. Jules, P.-Y. Bony, H. Kawashima, W. Gao, T. Kohoutek, T. Suzuki, Y. Ohishi, and F. Smektala, "Mid-infrared 2000-nm bandwidth supercontinuum generation in suspended-core microstructured sulfide and tellurite optical fibers," Opt. Express **20**, 27083–27093 (2012).
19. M. Belal, L. Xu, P. Horak, L. Shen, X. Feng, M. Ettabib, D. J. Richardson, P. Petropoulos, and J. H. V. Price, "Mid-infrared supercontinuum generation in suspended core tellurite microstructured optical fibers," Opt. Lett. **40**, 2237–2240 (2015).
20. T. Cheng, L. Zhang, X. Xue, A. Wnag, D. Deng, T. Suzuki, and Y. Ohishi, "Broadband cascaded four-wave mixing and supercontinuum generation in a tellurite microstructured optical fiber pumped at 2 μm," Opt. Express **23**, 4125–4134 (2015).
21. J. Picot-Clemente, C. Strutynski, F. Amrani, F. Désévédavy, J.-C. Jules, G. Gadret, D. Deng, T. Cheng, K. Nagasaka, Y. Ohishi, B. Kibler, and F. Smektala, "Enhanced supercontinuum generation in tapered tellurite suspended core fiber," Opt. Commun. **354**, 374–379 (2015).
22. P. Domachuk, N. A. Wolchover, M. Cronin-Golomb, A. Wang, A. K. George, C. M. B. Cordeiro, J. C. Knight, and F. G. Omenetto, "Over 4000 nm bandwidth of mid-IR supercontinuum generation in sub-centimeter segments of highly nonlinear tellurite PCFs," Opt. Express **16**, 7161–7168 (2008).
23. R. Thapa, D. Rhonehouse, D. Nguyen, K. Wiersma, C. Smith, J. Zong, and A. Chavez-Pirson, "Mid-IR supercontinuum generation in ultra-low loss, dispersion-zero shifted tellurite glass fiber with extended coverage beyond 4.5 μm," Proc. SPIE **8898**, 889808 (2013).
24. S. Kedenburg, T. Steinle, F. Mörz, A. Steinmann, D. Nguyen, D. Rhonehouse, J. Zong, A. Chavez-Pirson, and H. Giessen, "Solitonic supercontinuum of femtosecond mid-IR pulses in W-type index tellurite fibers with two zero dispersion wavelengths," APL Photonics **1**, 086101 (2016).
25. C. Strutynski, J. Picot-Clémente, A. Lemière, P. Froidevaux, F. Désévédavy, G. Gadret, J.-C. Jules, B. Kibler, and F. Smektala, "Fabrication and characterization of step-index tellurite fibers with varying numerical aperture for near- and mid-infrared nonlinear optics," J. Opt. Soc. Am. B **33**, D12–D18 (2016).
26. M. Boivin, M. El-Amraoui, S. Poliquin, R. Vallée, and Y. Messaddeq, "Advances in methods of purification and dispersion measurement applicable to tellurite-based glasses," Opt. Mater. Express **6**, 1079–1086 (2016).
27. M. O'Donnell, K. Richardson, R. Stolen, A. Seddon, D. Furniss, V. Tikhomirov, C. Rivero, M. Ramme, R. Stegeman, G. Stegeman, M. Couzi, and T. Cardinal, "Tellurite and fluorotellurite glasses for fiber optic Raman amplifiers: Glass characterization, optical properties, Raman gain, preliminary fiberization, and fiber characterization," J. Am. Ceram. Soc. **90**, 1448–1457 (2007).
28. I. Savelii, F. Désévédavy, J.-C. Jules, G. Gadret, J. Fatome, B. Kibler, H. Kawashima, Y. Ohishi, and F. Smektala, "Management of OH absorption in tellurite optical fibers and related supercontinuum generation," Opt. Mater. **35**, 1595–1599 (2013).
29. C. Strutynski, P. Froidevaux, F. Désévédavy, J.-C. Jules, G. Gadret, A. Bendahmane, K. Tarnowski, B. Kibler, and F. Smektala, "Tailoring supercontinuum generation and four-wave mixing beyond 2 μm in step-index tellurite fibers," Opt. Lett. **42**, 247–250 (2017).
30. C. Strutynski, J. Picot-Clemente, F. Désévédavy, J.-C. Jules, G. Gadret, B. Kibler, and F. Smektala, "Compact supercontinuum sources based on tellurite suspended core fibers for absorption spectroscopy beyond 2 μm," Laser Phys. Lett. **13**, 075402 (2016).
31. J. M. Dudley, G. Genty, and S. Coen, "Supercontinuum generation in photonic crystal fiber," Rev. Mod. Phys. **78**, 1135–1184 (2006).
32. M. D. O'Donnell, K. Richardson, R. Stolen, C. Rivero, T. Cardinal, M. Couzi, D. Furniss, and A. B. Seddon, "Raman gain of selected tellurite glasses for IR fibre lasers calculated from spontaneous scattering spectra," Opt. Mater. **30**, 946–951 (2008).
33. C. Xia, M. Kumar, M.-Y. Cheng, O. P. Kulkarni, M. N. Islam, A. Galvanauskas, F. L. Terry, M. J. Freeman, D. A. Nolan, and W. A. Wood, "Supercontinuum generation in silica fibers by amplified nanosecond laser diode pulses," IEEE J. Sel. Top. Quantum Electron. **13**, 789–797 (2007).
34. F. Mörz, T. Steinle, A. Steinmann, and H. Giessen, "Multi-watt femtosecond optical parametric master oscillator power amplifier at 43 MHz," Opt. Express **23**, 23960–23967 (2015).
35. T. Steinle, F. Mörz, A. Steinmann, and H. Giessen, "Ultra-stable high average power femtosecond laser system tunable from 1.33 to 20 μm," Opt. Lett. **41**, 4863–4866 (2016).
36. A. Steinmann, B. Metzger, R. Hegenbarth, and H. Giessen, "Compact 7.4 W femtosecond oscillator for white-light generation and nonlinear microscopy," in *Conference on Lasers and Electro-Optics (CLEO)*, OSA Technical Digest (CD) (Optical Society of America, 2011), paper CThAA5.